Scientific Research Publishing

Open Journal of Geology, 2026, 16(2), 85-103
https://www.scirp.org/journal/ojg
ISSN Online: 2161-7589
ISSN Print: 2161-7570

Petrology and Geochemistry of Precambrian Mafic and Ultramafic Rocks from North Devanahalli, Bangalore Rural, Karnataka, Southern India

Priyanka Harohalli Subramani, Shadaksharaswamy Nagabhushan

Department of Geology, Bangalore University, Bangalore, India
Email: priyankahsubramani@gmail.com

How to cite this paper: Harohalli Subramani, P. and Nagabhushan, S. (2026) Petrology and Geochemistry of Precambrian Mafic and Ultramafic Rocks from North Devanahalli, Bangalore Rural, Karnataka, Southern India. *Open Journal of Geology*, **16**, 85-103.
https://doi.org/10.4236/ojg.2026.162006

Received: January 5, 2026
Accepted: February 7, 2026
Published: February 10, 2026

Abstract

The Archaean crust of the eastern Dharwar Craton preserves important records of early mantle-derived magmatism and crustal evolution. Mafic and ultramafic rocks occurring in the Precambrian terrain of North Devanahalli Taluk, Bangalore Rural District, southern India, form a significant component in this regard. These rocks occur as enclaves, lenses, and intrusive bodies within the Peninsular Gneissic Complex and are spatially associated with high-grade metamorphic lithologies. The present study integrates field observations, petrographic investigations, and whole-rock geochemical analyses of representative mafic and ultramafic samples to constrain their petrogenesis and tectonic affinity. Petrographic characteristics reveal relict magmatic textures such as gabbroic and poikilitic fabrics, overprinted by granoblastic textures developed during amphibolite to lower granulite facies metamorphism. Geochemical data indicate tholeiitic to komatiitic affinity, marked by enrichment of compatible elements (Ni, Cr, Co, V) and weakly fractionated rare earth element patterns. These features suggest derivation from mantle-derived magmas followed by limited fractional crystallization and minor crustal interaction. The mafic-ultramafic rocks of the study area represent remnants of Archaean magmatic activity associated with early crust-mantle differentiation processes in the eastern Dharwar Craton.

Keywords

Mafic Rocks, Ultramafic Rocks, Petrography, Geochemistry, Archaean, Eastern Dharwar Craton

1. Introduction

Archaean cratons worldwide provide invaluable insights into the processes responsible for early continental crust formation and stabilization. Mafic and ultramafic rocks are particularly significant in this context, as they represent direct products of mantle melting and preserve geochemical signatures of high-temperature magmatic regimes characteristic of the early Earth [1]-[3]. In the Indian shield, the Dharwar Craton is one of the best-preserved Archaean terranes, comprising greenstone belts, TTG gneisses, granitoids, and associated mafic-ultramafic complexes [4]-[6].

The present study focuses on the mafic and ultramafic rocks occurring within the Precambrian crystalline terrain of Devanahalli Taluk, Bangalore Rural District, southern India. These rocks are spatially associated with the Peninsular Gneissic Complex (PGC) and belong to the Archaean [3] [7] [8] supracrustal assemblages of the southern Dharwar Craton. Despite their petrological importance, these bodies have received relatively limited integrated petrographic and geochemical attention at a local scale. The present work aims to i) document the petrographic characteristics of the mafic and ultramafic rocks, ii) evaluate their major, trace, and rare earth element geochemistry, and iii) interpret their petrogenesis and tectonic significance within the Archaean evolution of southern India.

2. Geological Setting

The study area (**Figure 1**) forms part of the eastern Dharwar Craton and is underlain predominantly by the Peninsular Gneissic Complex, which represents polyphase Archaean crustal evolution. The gneissic basement encloses discontinuous enclaves of supracrustal rocks correlated with the Sargur Group (>3000 Ma), along with younger granitoid intrusions. The terrain has undergone multiple episodes of deformation and metamorphism, reaching amphibolite to granulite facies conditions [8]-[10]. Mafic and ultramafic rocks occur as lenses, enclaves, and dyke-like bodies within the gneisses. Field relationships commonly show sharp intrusive contacts and locally preserved chilled margins, indicating the emplacement of hot mafic magmas into cooler continental crust. These bodies are spatially associated with amphibolites, migmatitic gneisses, and granitoids, reflecting a complex interplay of magmatism, metamorphism, and deformation during Archaean crustal growth [11] [12].

The rocks of the present study area are comparable in field characteristics and lithological association to other Archaean mafic-ultramafic occurrences reported from southern India. In the study area, altered ultramafic rocks (**Figure 2**) are present within the gneiss or leucogneiss. Ultramafic rocks are represented exclusively in the form of gabbro. Two distinct varieties of gabbro are identified: mono-gabbro and olivine-bearing gabbro (**Figure 3**) and they occur as intrusions into the PGC. They exhibit an intrusive nature with the host rock characterized by well-defined contacts and chilled margins. The prominent occurrence of gabbro is observed in the northwest of Tubgere and continues towards the

eastern part. It occurs in the form of dykes (Figure 4). Diorite occurs as coarse- to medium-grained, intermediate intrusive bodies with sharp contacts against the surrounding granitic gneisses within the study area. The outcrops are generally massive, moderately jointed, and exhibit characteristic grey to dark grey coloration on fresh surfaces, turning light grey to brown upon weathering (Figure 5).

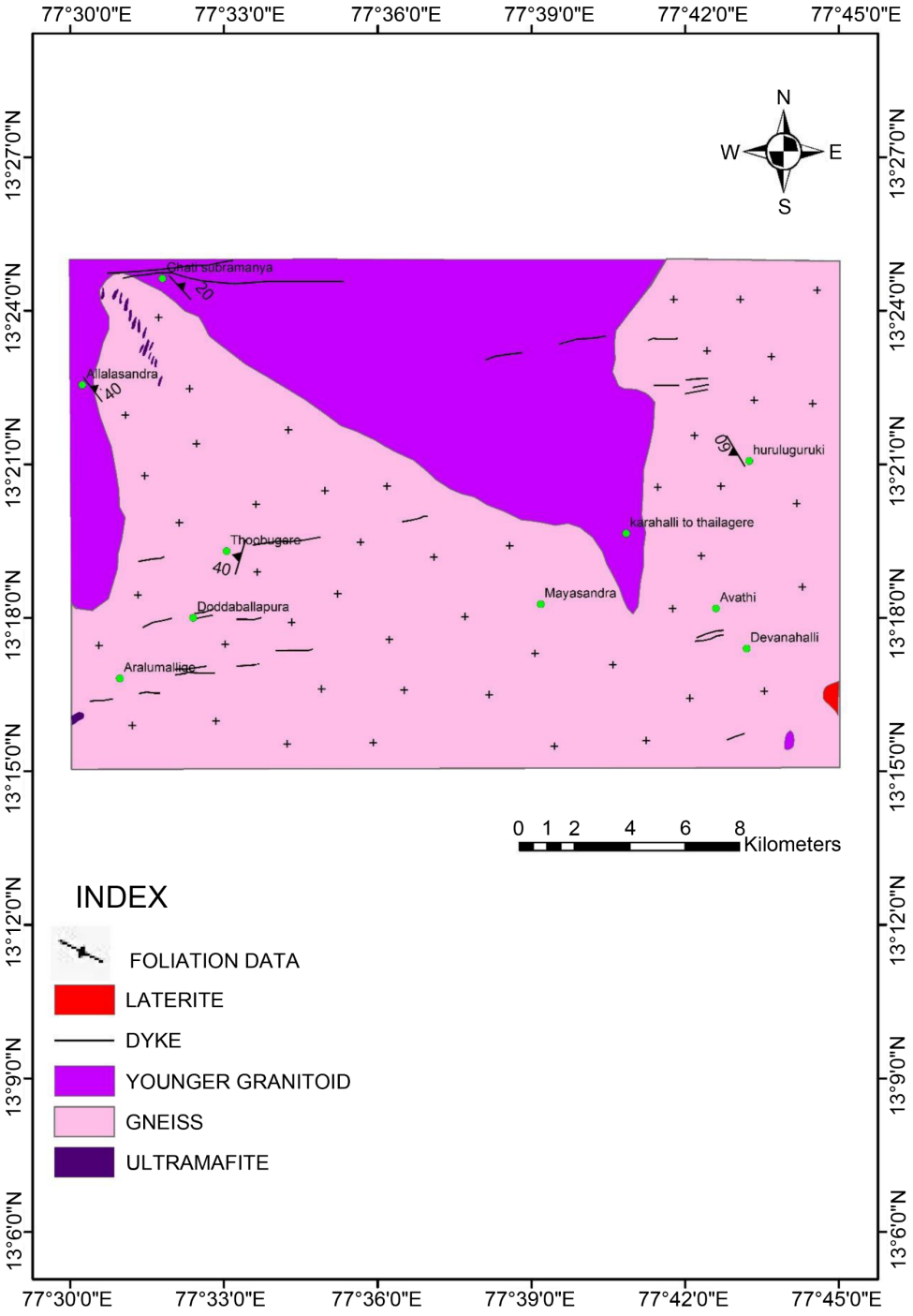

Figure 1. Geological map of the study area.

Figure 2. Field photo of altered ultramafic rocks within gneiss.

Figure 3. Field photo of highly weathered olivine gabbro.

Figure 4. A field photograph shows a gabbroic dyke with a sharp contact and chilled margin.

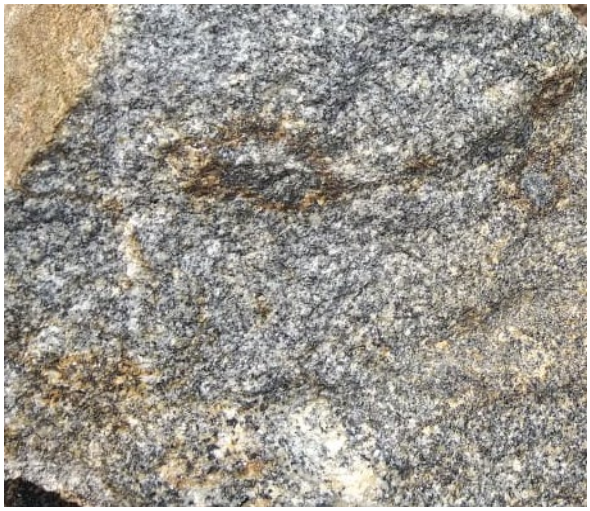

Figure 5. A field photograph of weathered diorite rock.

3. Materials and Methods

Mafic and ultramafic rock samples were systematically collected from multiple locations within the study area during field investigations. Sampling focused on seven representative samples, which were selected, and thin sections were prepared to study the textural and mineralogical characteristics. Sample preparation involved initial cleaning and trimming of altered surfaces, followed by crushing using a steel jaw crusher and pulverization in an agate mill to avoid metal contamination. Representative powdered samples were used for whole-rock geochemical analyses. These samples were analyzed using XRF, ICP-OES, and ICP-MS to determine the major, minor, trace, and rare earth elements (Tables 1-5). The resulting data were subsequently utilized to understand geochemical evolution. Major element concentrations were determined by Borate Fusion Bead preparation followed by 4.0KW WD XRF at Shiva Analyticals (India) Private Ltd., Bangalore. Trace element concentrations were determined using Inductively Coupled Plasma Optical Emission Spectrometry (ICP-OES), and rare earth elements were analyzed by Inductively Coupled Plasma Mass Spectrometry (ICP-MS) at Shiva Analyticals (India) Private Ltd., Bangalore. Analytical precision was monitored using international rock standards, and repeated analyses of selected samples were done for analytical uncertainties, which are generally better than ±2% for major oxides and ±5% for trace elements.

Table 1. Major element analysis data.

Sample No	MB3	TU3	KG2	AS1	AS2	MG1	MRB1
SiO_2	47.74	47.7	50.52	51.36	50.1	60.23	52.18
Al_2O_3	14.54	12.29	14.11	5.4	13.65	15.14	14.53
Fe_2O_3	15.11	19.13	14.09	11.85	16.6	8.11	11.2
MgO	5.88	4.47	5.88	25.13	4.53	2.93	5.75

Continued

CaO	9.09	8.94	9.8	4.66	9.01	5.9	9.8
Na_2O	2.99	2.52	2.33	0.08	2.58	4.21	4.29
K_2O	1.61	0.99	0.76	0.05	0.94	1.46	0.64
TiO_2	1.25	2.72	1.09	0.18	1.66	0.99	0.63
P_2O_5	0.16	0.36	0.14	0.05	0.22	0.25	0.21
MnO	0.21	0.17	0.16	0.08	0.18	0.07	0.15
Cr_2O_3	0.05	0.05	0.05	0.66	0.05	0.05	0.05
BaO	0.05	0.05	0.05	0.05	0.05	0.05	0.05
LOI	0.97	<0.1	0.83	0.43	<0.1	0.46	0.51
Total	99.65	99.39	99.81	99.98	99.57	99.85	99.99

Table 2. Trace element data.

Sample No	MB3	TU3	KG2	AS1	AS2	MG1	MRB1
Sr	20.24	29.97	29.44	12.92	30.85	24.21	17.43
Zr	47.5	43.73	41.89	78.42	41.57	45.04	51.92
V	23.01	19.92	22.74	8.47	20.88	17.17	21.37
Sn	9.25	6.38	5.93	0.19	6.69	13.57	9.28
Mo	112.55	99.01	109.22	86.85	108.17	163.11	106.01
Ga	3.07	2.54	3.48	7.55	2.7	1.61	2.75
Y	1.85	1.65	1.36	2.73	1.49	1.14	0.73
Nb	20.24	29.97	29.44	12.92	30.85	24.21	17.43
Cu	47.5	43.73	41.89	78.42	41.57	45.04	51.92
Pb	23.01	19.92	22.74	8.47	20.88	17.17	21.37
Zn	9.25	6.38	5.93	0.19	6.69	13.57	9.28
Ni	112.55	99.01	109.22	86.85	108.17	163.11	106.01
Co	3.07	2.54	3.48	7.55	2.7	1.61	2.75
Cd	1.85	1.65	1.36	2.73	1.49	1.14	0.73
Sb	20.24	29.97	29.44	12.92	30.85	24.21	17.43
Bi	47.5	43.73	41.89	78.42	41.57	45.04	51.92
Ag	23.01	19.92	22.74	8.47	20.88	17.17	21.37

Table 3. Rare earth element concentrations.

Sample No	MB3	TU3	KG2	AS1	AS2	MG1	MRB1
La	7.03	18.28	9.34	1.39	13.14	40.67	14.57
Ce	16.2	41.95	21.38	2.79	29.97	82.18	25.37
Nd	10.53	23.99	11.46	1.56	16.99	36.99	14.02
Sm	3.07	5.96	2.97	<0.5	4.22	7.6	3.17
Eu	0.99	1.94	1.07	<0.5	1.46	1.99	0.89
Tb	0.59	1.13	0.69	<0.5	0.76	0.97	<0.5
Yb	3.7	4.73	3.09	0.53	4.35	4.23	2.46
Lu	0.51	0.65	<0.5	<0.5	0.6	0.53	<0.5

Table 4. Niggli value calculation.

Sample No	MB3	TU3	KG2	AS1	AS2	MG1	MRB1
al	20.24	29.97	29.44	12.92	30.85	24.21	17.43
fm	47.5	43.73	41.89	78.42	41.57	45.04	51.92
c	23.01	19.92	22.74	8.47	20.88	17.17	21.37
alk	9.25	6.38	5.93	0.19	6.69	13.57	9.28
Si	112.55	99.01	109.22	86.85	108.17	163.11	106.01
Mg	3.07	2.54	3.48	7.55	2.7	1.61	2.75
K	1.85	1.65	1.36	2.73	1.49	1.14	0.73
c/fm	0.48	0.46	0.54	0.11	0.50	0.38	0.41
c + fm	70.51	63.65	64.63	86.89	62.45	62.21	73.29

Table 5. CIPW norm calculation of gneissic rocks.

Sample No	MB3	TU3	KG2	AS1	AS2	MG1	MRB1
Quartz	1.26	9.39	9.49	5.26	10.52	16.02	2.01
Orthoclase	9.51	5.91	4.55	0.3	5.61	8.69	3.78
Albite	25.3	21.49	19.97	0.76	21.92	35.88	36.55
Anorthite	21.5	19.42	26.07	14.37	23	18.24	18.61
Nepheline	-	-	-	-	-	-	-
Diopside	14.82	10.91	14.78	6.54	11.99	4.99	21.28
Hypersthene	7.78	6.15	7.97	60.29	5.77	5.04	4.56
Olivine	0	0	0	0	0	0	0

Continued

Ilmenite	0.45	0.36	0.34	0.19	0.38	0.15	0.32
Apatite	0.37	0.83	0.32	0.12	0.51	0.58	0.48
Titanite	2.49	6.26	2.26	0.19	3.6	2.26	1.13
Hematite	15.28	19.18	14.25	11.99	16.69	8.17	11.27
Zircon	-	0.03	-	-	-	-	-

Thin sections were prepared for all samples and examined using a polarizing microscope to document mineralogical assemblages and textural relationships.

4. Petrography

Mineral identification in the present study is primarily based on detailed optical petrography using transmitted light microscopy. Diagnostic optical properties such as birefringence, extinction angle, pleochroism, twinning, and textural relationships were used for mineral determination.

Petrographic studies indicate that the ultramafic rocks are represented mainly by gabbro, meta-gabbro, olivine-bearing gabbro, and altered ultramafite. Primary igneous textures are variably preserved, although most samples exhibit significant metamorphic recrystallization.

Gabbros display medium- to coarse-grained gabbroic textures composed predominantly of augite and plagioclase. Plagioclase commonly shows polysynthetic twinning and partial saussuritization, whereas augite exhibits inclined extinction and is locally replaced by hornblende (Figure 6(a)). In some samples, micrographic and intergranular textures (Figure 6(b)) suggest crystallization from a tholeiitic magma.

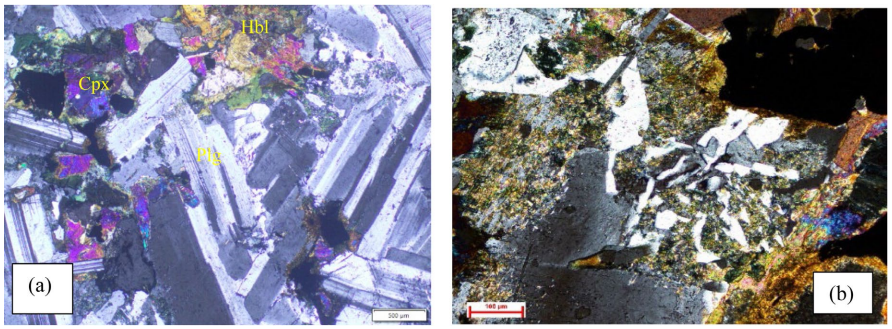

Figure 6. Microphotographs of gabbroic rock. (a) Plagioclase laths with triple junctions, intergrown with clinopyroxene and minor hornblende under crossed nicols. (b) MGP texture with primary quartz intergrown with feldspar in gabbro under crossed nicols.

Meta-gabbro generally consists of inequigranular, euhedral to subhedral grains, and shows a granular to granoblastic texture. Plagioclase is seen as plates with polysynthetic twinning and is seen altering into epidote. All the epidotes are deformed and metamorphosed. Foliated to schistose structure is well developed

(Figure 7(a)) in some samples. Chloritization of biotite and sericitization of plagioclase and hornblende are observed. Sphene occurs as euhedral grains with high relief and interference color (Figure 7(b)).

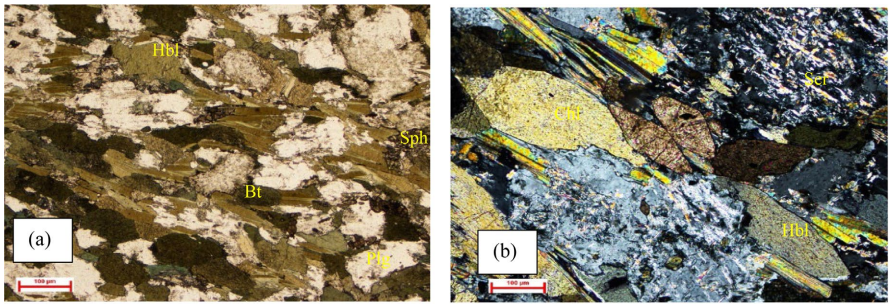

Figure 7. (a) Hornblende-biotite-plagioclase-sphene association in meta-gabbro showing prominent foliation under plane-polarized light. (b) Chloritization of biotite, sericitization of plagioclase, and hornblende in meta-gabbro under crossed nicols. Note the presence of euhedral grains of sphene.

Olivine-bearing gabbros are characterized by poikilitic textures, where olivine and pyroxene grains are enclosed within plagioclase (Figure 8(a)). Olivine is frequently serpentinized (Figure 8(b)), and pyroxenes show marginal alteration to amphibole and chlorite. The pyroxene-plagioclase-phlogopite association shows cumulous and intercumulous textures (Figure 9(a)).

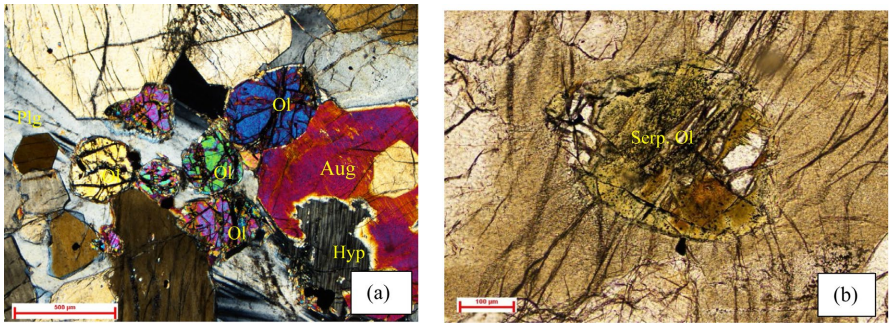

Figure 8. Microphotograph of olivine-gabbro. (a) Olivine-augite-hypersthene-plagioclase showing poikilitic texture under crossed nicols. (b) Serpentinized olivine showing poikilitic texture in olivine-gabbro under plane-polarized light.

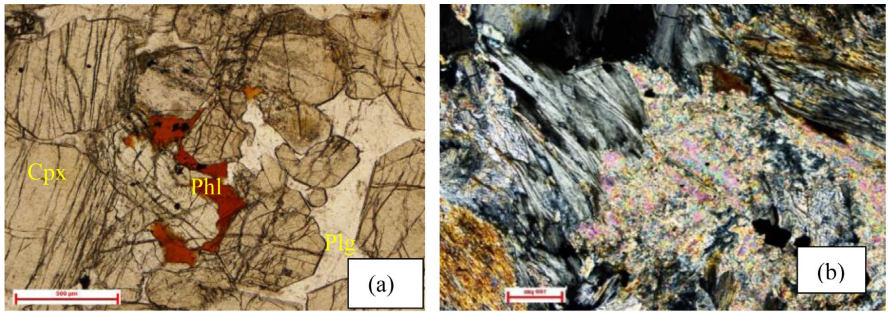

Figure 9. (a) Pyroxene-plagioclase-phlogopite association in olivine-gabbro showing cumulus and intercumulus texture under plane polarized light. (b) Tremolite, talc, and chlorite in meta-ultramafite under crossed nicols.

Meta-ultramafite consists of relict olivine and pyroxene assemblages replaced by tremolite, talc, and Mg-rich chlorite (Figure 9(b)), indicating subsequent hydration.

Diorite in the study area exhibits intergranular to gabbroic texture and shows evidence of intersertal fabric. Myrmekitic intergrowth of quartz and plagioclase feldspars is observed (Figure 10). Plagioclase and hornblende are associated with biotite. Biotite shows effects of chloritization (Figure 11(a), Figure 11(b)).

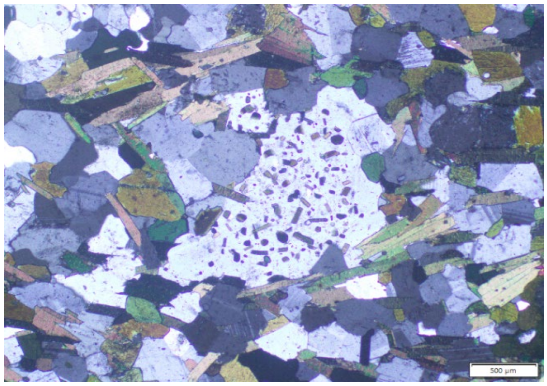

Figure 10. Myrmekitic intergrowth of quartz and plagioclase feldspars under crossed nicols.

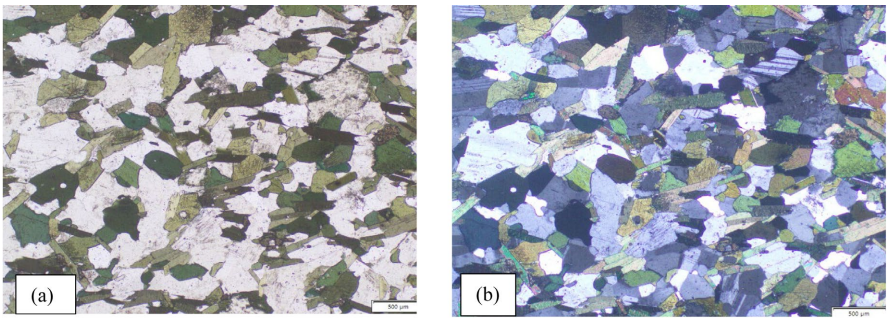

Figure 11. (a) Plagioclase-hornblende-biotite association with chloritization in diorite under plane polarized light. (b) Plagioclase-hornblende-biotite association with chloritization in diorite under crossed nicols.

Metamorphic Overprint

The widespread development of hornblende, epidote, chlorite, and granoblastic textures suggests that the mafic-ultramafic rocks were subjected to amphibolite to lower granulite facies metamorphism. Deformation-related features such as foliation, recrystallized grain boundaries, and mineral alignment reflect regional tectono-thermal events affecting the Archaean basement.

5. Geochemistry

It is important to note that the study area has experienced amphibolite- to lower granulite-facies metamorphism, and many samples exhibit mineralogical evidence of alteration such as sericitization, chloritization, and saussuritization. Consequently, large ion lithophile elements (LILE) such as Na, K, and Ca may have

experienced partial mobility during post-magmatic processes. Therefore, greater emphasis is placed on relatively immobile elements (e.g., Ti, Zr, Nb, Y, Cr, Ni, REE) when interpreting classification diagrams and petrogenetic trends, while alkali-based plots (AFM diagrams) are interpreted with caution.

The mafic and ultramafic rocks exhibit SiO_2 contents ranging approximately from 48 to 60 wt.%, with MgO contents varying widely, reaching high values in ultramafic samples. Al_2O_3, Fe_2O_3, CaO, and TiO_2 show moderate variation, reflecting mineralogical control by olivine, pyroxene, and plagioclase fractionation.

The chemistry of ultramafic rocks is plotted on the MgO-CaO-/Al_2O_3 diagram (**Figure 12**) of Viljoen and Viljoen (1969), and the plots show a clear grouping and fall close to the tholeiitic field, with one plot falling in the komatiitic field. The plots show a similarity with those of the Sanspruit and Geluk-type komatiites of the Onverwacht Group of Barberton Mountain Land of South Africa [13] and the Banasandra area, Kibbanahalli arm [12], and Honnebetta area and Nagamangala schist belt [14].

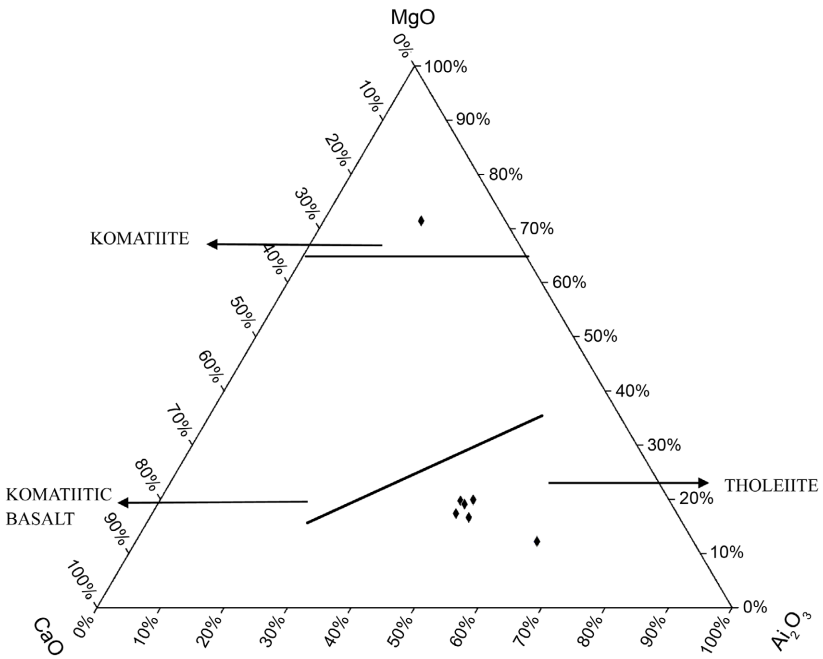

Figure 12. Plots of ultramafic rocks CaO-MgO-Al_2O_3 diagram after Viljoen & Viljoen 1969.

On the Niggli al-alk-c + fm diagram, plots of ultramafic rocks fall well within the igneous field (**Figure 13**).

On the classical cation (FeO + Ti)-Al-MgO diagram after Jenson (1976) (**Figure 14**), all the plots fall in the Fe tholeiite field except for one, which falls in the komatiite field. On the A-F-M diagram after Irwin and Bargar (1971) (**Figure 15**), the ultramafic rock plots show a tholeiitic trend. When plotted on the MgO-CaO-/Al_2O_3 diagram after Muir (1979) (**Figure 16**), one plot falls in the peridotitic komatiite field and remarkably shows an aluminum-depleted nature relative to cal-

cium, whereas other plots fall near the CaO-Al_2O_3 tie line. On Na_2O+K_2O vs SiO_2 diagram (Figure 17) the samples plot in the tholeiitic field except for one, which falls in the alkaline field. On the TiO_2-MnO-P_2O_5 diagram after Mullen (Figure 18), most of the plots fall in the IAT field, a few fall in the CAB field, and one plot falls in the OIT field. On the CaO/Al_2O_3-SiO_2-CaO diagram after Schweitzer & Kroner (1985) (Figure 19), all the plots fall in the altered field.

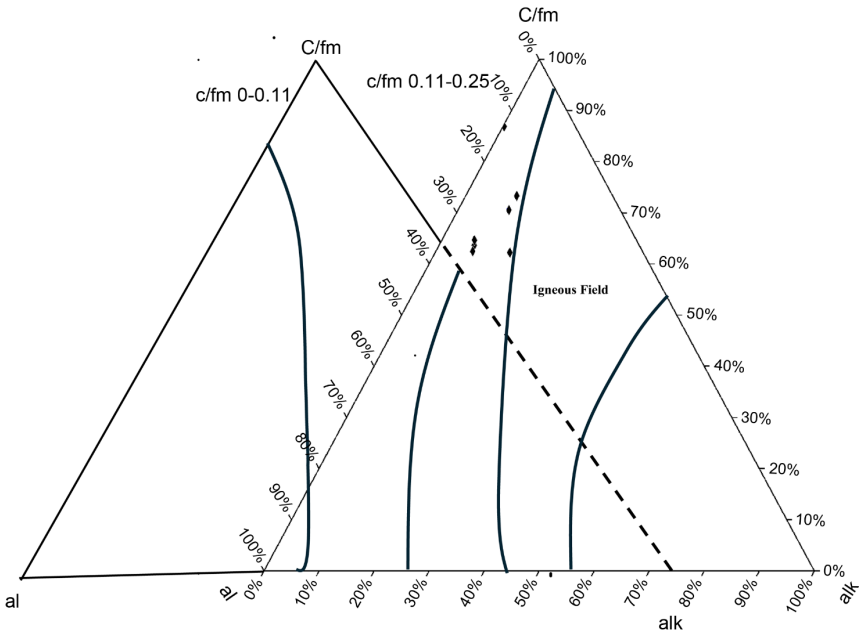

Figure 13. Niggli al-alk-c/fm for the ultramafic rocks.

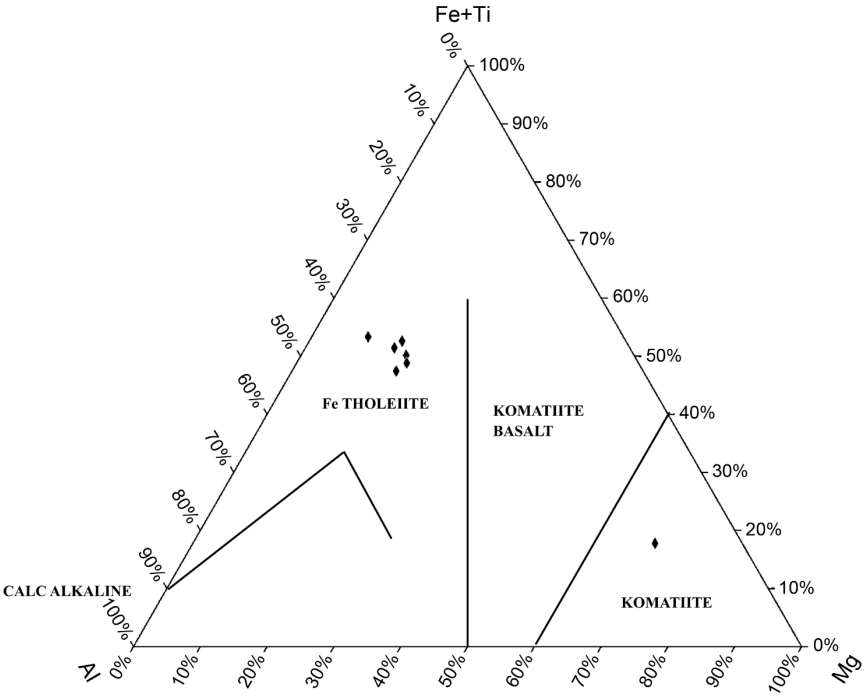

Figure 14. Plots of the ultramafic rocks diagram after Jensen (1976).

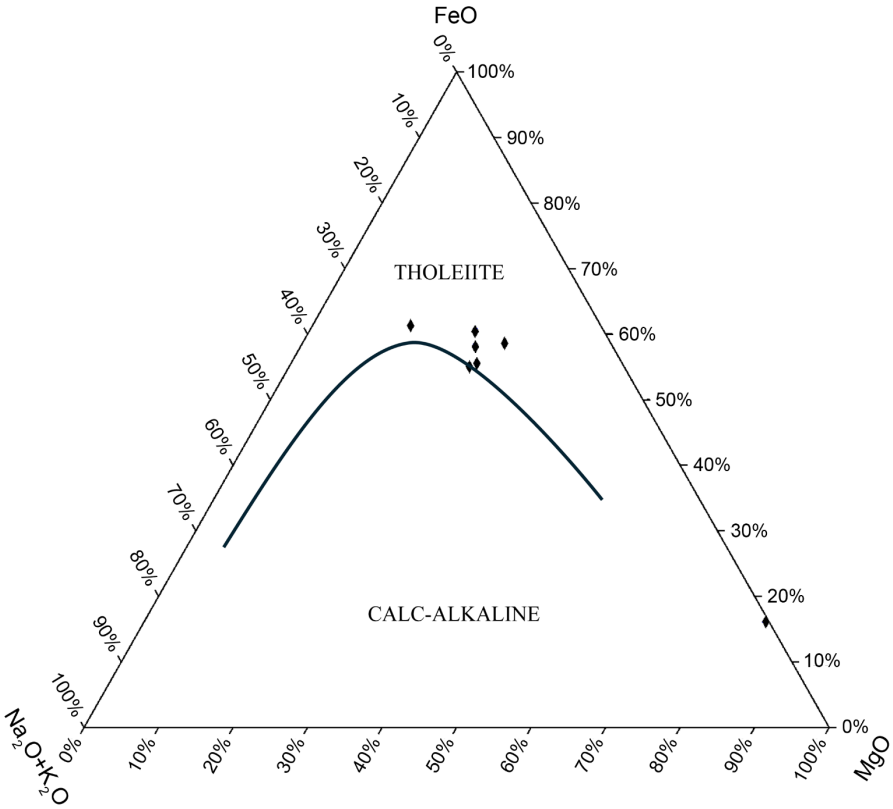

Figure 15. Plots of ultramafic AFM diagram after Irwin and Baragar (1971).

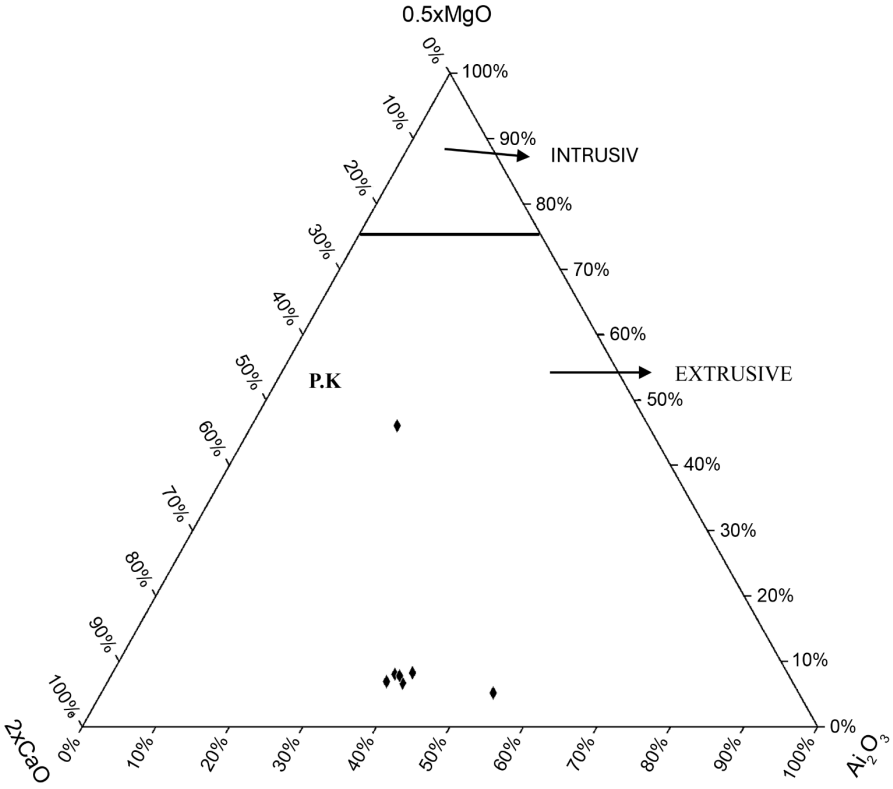

Figure 16. Plots of ultramafic rock diagrams after Muir (1979).

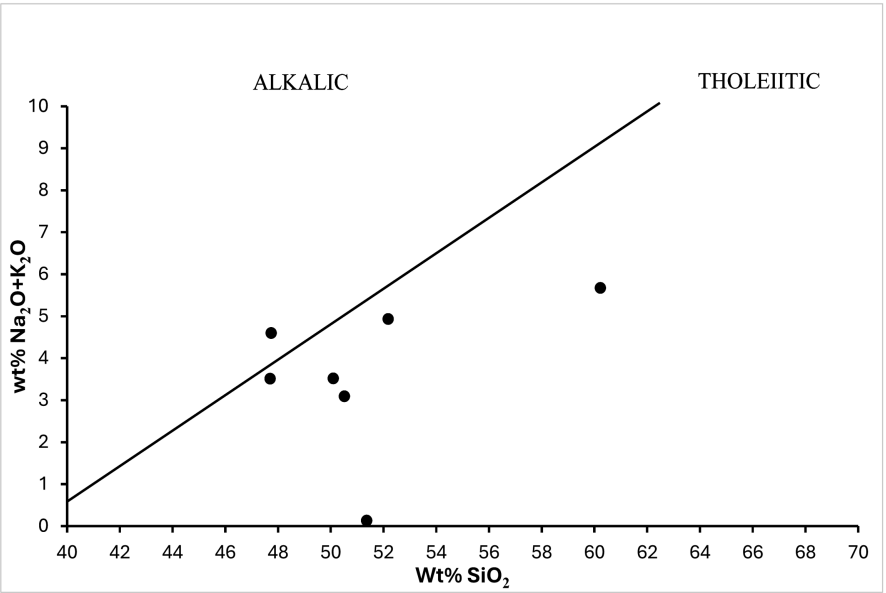

Figure 17. Alkali-silica diagram.

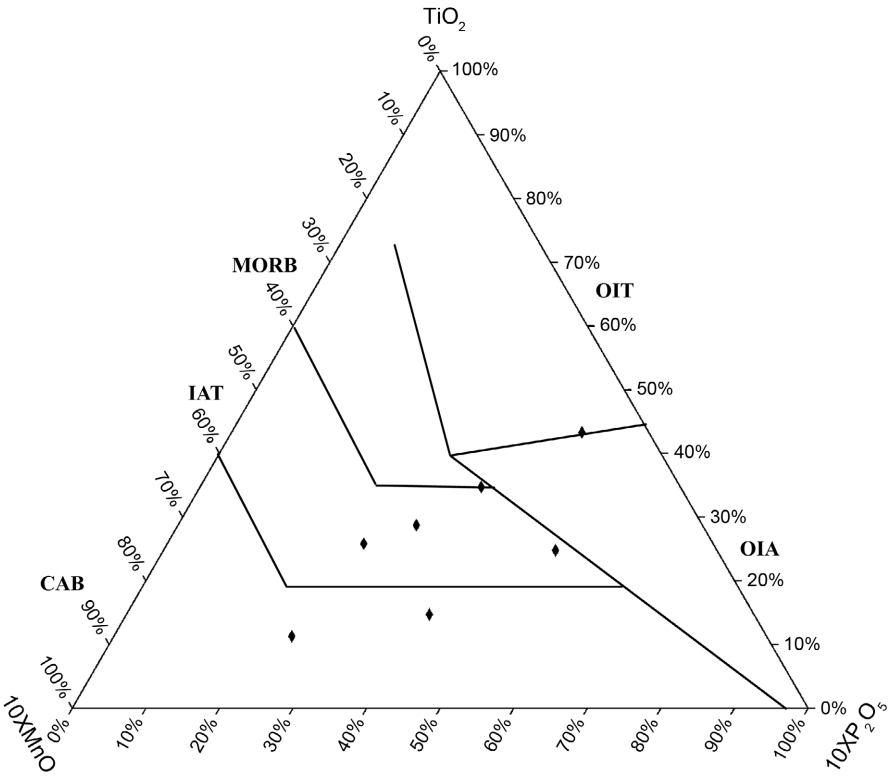

Figure 18. Plots of ultramafic rocks diagram after Mullen (1983).

The trace and REE data of ultramafic rocks are given in Table 2, Table 3. Trace element data reveal enrichment of compatible elements such as Ni, Cr, Co, and V, consistent with a mantle source. The ultramafic and mafic rocks of the area show characteristic enrichment in certain trace elements like Ni & V. Ni ranges from 36 to 773 ppm in the ultramafic rocks of the study area. On the MgO vs major oxides

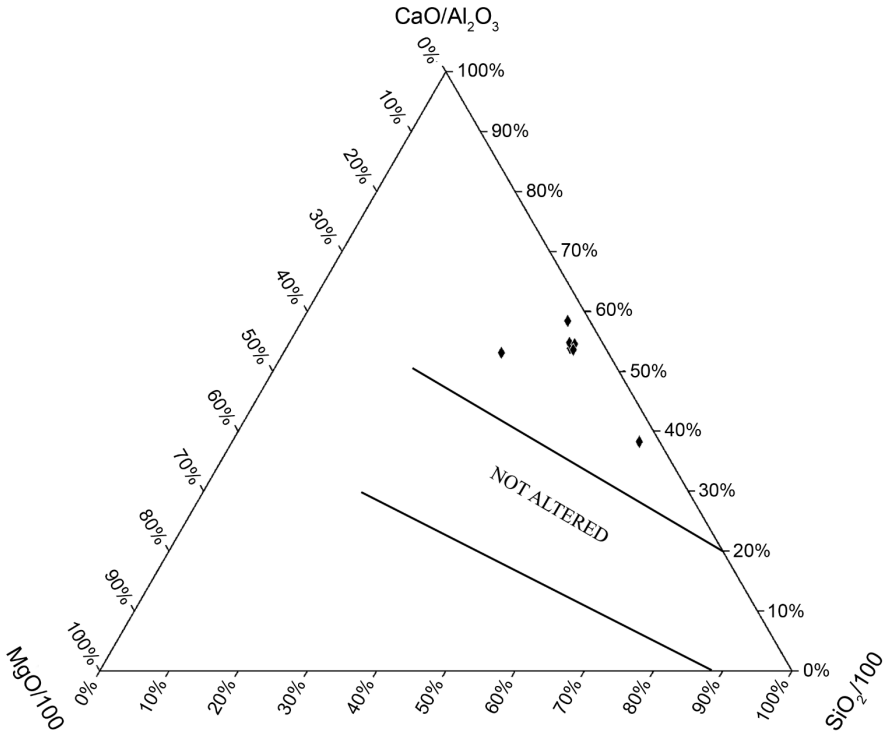

Figure 19. Plot of ultramafic rocks diagram after Schweitzer & Kroner (1985).

diagram (Figure 20), no trend is observed. Na_2O, K_2O, and CaO do not show any trend, indicating their mobility during metamorphism and alteration. On the MgO-Ni diagram (Figure 21) the plots show a positive trend. The cobalt concentration ranges from 32.74 to 87.41 ppm, which is almost similar to the reported values for ultramafic rocks from other Archaean terrains [15]. V content ranges from 59 to 537 ppm and is mainly concentrated in magnetite and to a lesser extent in pyroxene. Nickhold and Allen (1956) have shown that vanadium is concentrated in the middle to late stages of fractional crystallization. The reported values of vanadium in ultramafic rocks elsewhere range from 150 to 400 ppm [7] [15]. Nickel concentrations reach several hundred ppm in ultramafic varieties, comparable with Archaean ultramafic rocks reported from other cratonic regions [16]-[18].

The REE distribution is extremely valuable in placing constraints on the origin of ultramafic and mafic magmas (Condie, 1981). REE data are presented in Table 3, and the plots are given in Figure 22. REE patterns show a lesser rate of fractionation. The REE patterns of the samples are greater. Chondrite-normalized REE patterns are characterized by weakly enriched light rare earth elements and a relatively flat heavy rare earth element distribution, with negligible Eu anomalies. Such patterns are typical of Archaean mafic-ultramafic rocks and suggest limited crustal contamination and moderate degrees of fractional crystallization.

Elemental variation trends provide insight into magmatic differentiation processes. The positive correlation between MgO and Ni suggests control by olivine fractionation during early crystallization stages. The weak negative correlations between MgO and Al_2O_3, CaO, and Fe_2O_3 are consistent with progressive fraction-

ation of clinopyroxene and plagioclase during magma evolution. The relatively flat chondrite-normalized REE patterns with minor LREE enrichment and absence of significant Eu anomalies suggest moderate degrees of fractional crystallization and limited plagioclase accumulation or removal. Collectively, these trends support derivation from mantle-derived magmas that experienced limited crystal fractionation prior to emplacement.

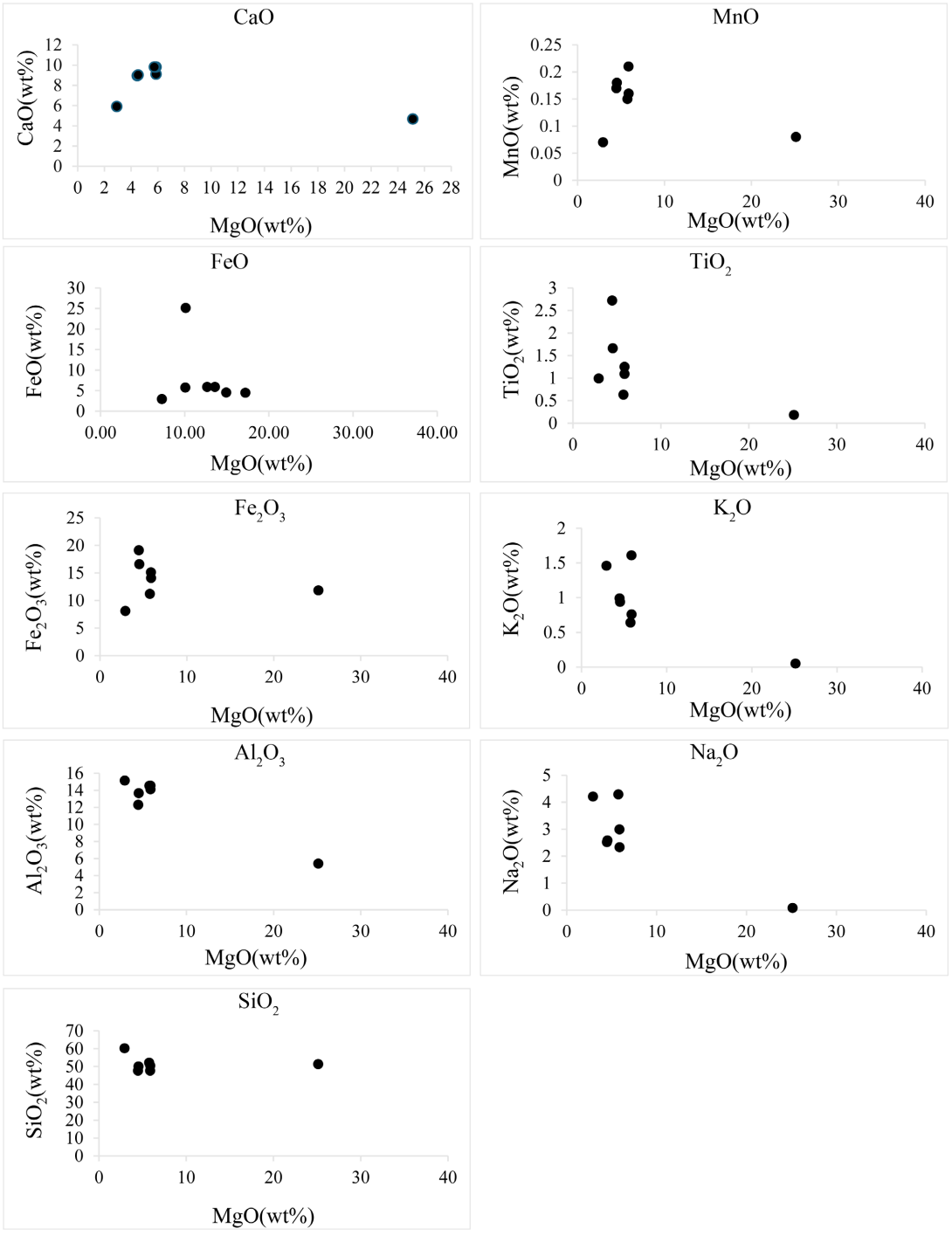

Figure 20. MgO versus major oxide diagram for ultramafic rocks.

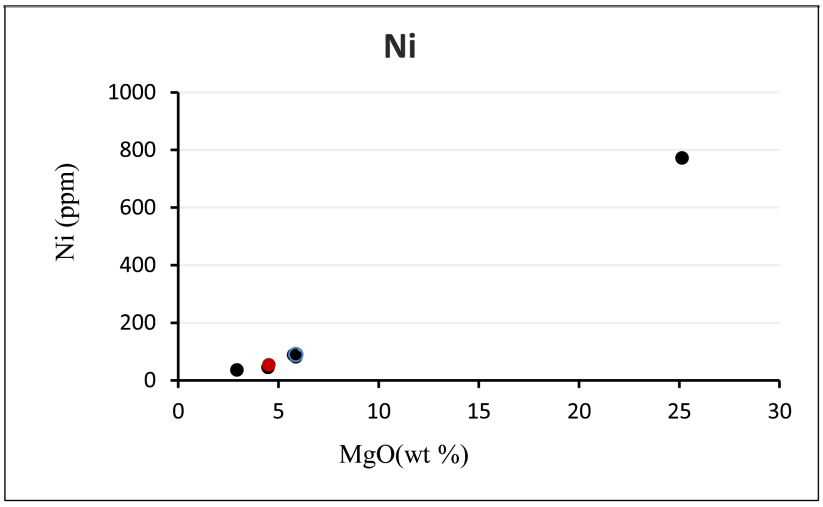

Figure 21. MgO versus Ni diagram for ultramafic rocks.

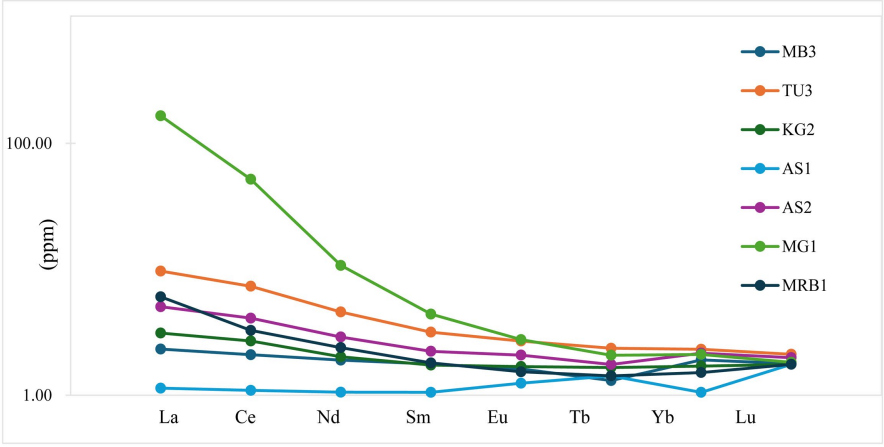

Figure 22. Rare earth element pattern for ultramafic rocks (Taylor and McLennan).

Petrogenesis and Tectonic Implications

The integrated petrographic and geochemical data set suggests that the mafic and ultramafic rocks of the North Devanahalli region originated from mantle-derived tholeiitic to locally komatiitic magmas. High MgO contents and enrichment of compatible elements such as Ni and Cr, particularly the positive correlation between MgO and Ni, indicate significant involvement of olivine in the early crystallization history. This relationship supports derivation from relatively primitive magmas rather than highly evolved compositions.

The weak fractionation of rare earth elements, absence of pronounced Eu anomalies, and relatively flat heavy REE patterns indicate moderate degrees of partial melting of a mantle source with limited crustal contamination. These features argue against extensive fractional crystallization or assimilation processes. Furthermore, the immobile trace element characteristics (e.g., Ti, Zr, Nb, Y) display compositions broadly comparable with Archaean tholeiitic to komatiitic suites reported from other parts of the Dharwar Craton and other greenstone belts.

The presence of komatiitic affinities in one sample implies locally elevated mantle temperatures during magma generation, consistent with geodynamic models for the Archaean Earth. The subsequent emplacement of these magmas into evolving continental crust was accompanied by regional deformation and amphibolite- to granulite-facies metamorphism, resulting in partial recrystallization of primary mineral assemblages while preserving key geochemical signatures. Therefore, the mafic-ultramafic rocks of North Devanahalli likely represent remnants of early Archaean mantle-derived magmatism linked to crust-mantle differentiation processes within the eastern Dharwar Craton [17]-[19].

6. Conclusions

1) Mafic and ultramafic rocks in the North Devanahalli Taluk occur as intrusive bodies and enclaves within the Peninsular Gneissic Complex.

2) Petrographic features preserve relict magmatic textures overprinted by amphibolite- to lower granulite-facies metamorphism.

3) Geochemical data indicate tholeiitic to komatiitic affinity with enrichment of compatible elements and weakly fractionated REE patterns.

4) The rocks were derived from mantle-derived magmas with limited crustal interaction.

5) These lithologies represent remnants of Archaean magmatism linked to early crust-mantle differentiation in the eastern Dharwar Craton.

Conflicts of Interest

The authors declare no conflicts of interest regarding the publication of this paper.

References

[1] Condie, K.C. (1981) Archean Greenstone Belts. Elsevier.

[2] Arndt, N.T. (1994) Chapter 1 Archean Komatiites. *Developments in Precambrian Geology*, **11**, 11-44. https://doi.org/10.1016/S0166-2635(08)70219-6

[3] Wilson, M. (1989) Igneous Petrogenesis. Unwin Hyman.

[4] Naqvi, S.M. and Rogers, J.J.W. (1987) Precambrian Geology of India. Oxford University Press.

[5] Ramakrishnan, M. and Vaidyanadhan, R. (2011) Geology of India. Geological Society of India.

[6] Moyen, J.F., Martin, H., Jayananda, M. and Auvray, B. (2003) Late Archaean Granites: A Typology Based on the Dharwar Craton (India). *Precambrian Research*, **127**, 103-123. https://doi.org/10.1016/s0301-9268(03)00183-9

[7] Sun, S.S. and Nesbitt, R.W. (1978) Geochemical Regularities of Archaean Ultramafic Rocks. *Geochimica et Cosmochimica Acta*, **42**, 1325-1342.

[8] Naha, K., Srinivasan, R. and Ghosh, S. (1991) Structural Evolution of the Peninsular Gneiss. *Precambrian Research*, **52**, 31-52.

[9] Radhakrishna, B.P. and Vasudev, V.N. (1977) The Early Precambrian of the Southern Indian Shield. *Journal Geological Society of India*, **18**, 525-541. https://doi.org/10.17491/jgsi/1977/181001

[10] Friend, C.R.L. and Nutman, A.P. (1992) Response of Granitoid Magmatism to Crustal Thickening. *Precambrian Research*, **55**, 281-300.

[11] Windley, B.F. (1977) The Evolving Continents. *Journal of the Geological Society*, **134**, 231-246.

[12] Srikantappa, C., Bose, S. and Janardhan, A.S. (1984) Ultramafic Complexes of Southern Karnataka. *Journal of the Geological Society of India*, **25**, 437-451.

[13] Jahn, B., Gruau, G. and Glikson, A.Y. (1982) Komatiites of the Onverwacht Group, S. Africa: REE Geochemistry, SM/ND Age and Mantle Evolution. *Contributions to Mineralogy and Petrology*, **80**, 25-40. https://doi.org/10.1007/bf00376732

[14] Devapriyan, G.V., Ananthar, T.R., Vidyadhar, K.T. and Raghu Nandan, K.R. (1994) Spinifex-Textured Peridotitic Komatiite from Honnabetta Area, Nagamangala Schist Belt, Karnataka. *Journal Geological Society of India*, **44**, 483-493. https://doi.org/10.17491/jgsi/1994/440502

[15] Gilkson, A.Y. (1982) Komatiites and Their Tectonic Setting. *Precambrian Research*, **17**, 1-26.

[16] Arth, J.G., *et al.* (1977) Rare Earth Element Systematics of Archaean Volcanic Rocks. *Geochimica et Cosmochimica Acta*, **41**, 157-170.

[17] Barker, F. and Arth, J.G. (1976) Generation of Trondhjemitic-Tonalitic Liquids and Archean Bimodal Trondhjemite-Basalt Suites. *Geology*, **4**, 596-600. https://doi.org/10.1130/0091-7613(1976)4<596:gotlaa>2.0.co;2

[18] Martin, H. (1987) Petrogenesis of Archaean TTG Suites. *Geology*, **15**, 544-547.

[19] Moyen, J. and Martin, H. (2012) Forty Years of TTG Research. *Lithos*, **148**, 312-336. https://doi.org/10.1016/j.lithos.2012.06.010